

# Lubricating and Waxy Esters. 4. Synthesis, Crystallization Behavior, Melt Behavior, and Flow Behavior of Linear Monoesters Incorporating 9-Decenol and 9-Decenoic Acid

Laziz Bouzidi,<sup>†</sup> Shaojun Li,<sup>†</sup> Steve Di Biase,<sup>‡</sup> Syed Q. Rizvi,<sup>‡</sup> and Suresh S. Narine<sup>\*,†</sup>

<sup>†</sup>Trent Centre for Biomaterials Research Departments of Physics & Astronomy and Chemistry, Trent University, 1600 West Bank Drive, Peterborough, Ontario K9J 7B8, Canada

<sup>‡</sup>Elevance Renewable Sciences, 175 East Crossroads Parkway, Suite F, Bolingbrook, Illinois 60440, United States

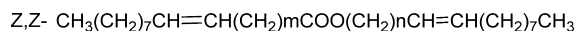
## S Supporting Information

**ABSTRACT:** Three pure jojoba wax-like esters (JLEs), i.e., octadec-9-enyl dec-9-enoate (JLE 28<sub>1</sub>), dec-9-enyl oleate (JLE 28<sub>2</sub>), and dec-9-enyl dec-9-enoate (JLE-20), were synthesized from fatty acids and fatty alcohols. Calorimetric, solid fat content evolution, and flow data were used to elucidate the phase behavior of the JLEs. It was clearly established that the length of the terminal alkyl chain and orientation of the linking group in the side chains of the bent-core molecules play an important role in the phase development of the JLEs and ultimately their physical properties. Measurable differences in all physical properties investigated were detected between the isomers based on the position of the ester group in the molecule, leading to informed choices on what isomer should be synthesized for similar monoesters for specific applications.

## 1. INTRODUCTION

Plant oils and their derivatives have been proven to be very good alternative renewable sources to petroleum for many applications including lubricants, waxes, and gels. Their many advantages include biodegradability,<sup>1</sup> low toxicity,<sup>2</sup> low volatility, and high viscosity indices.<sup>3</sup> Jojoba oil is particularly interesting because it is composed of a variety of monoesters (Scheme 1), which are believed to be the source of its unique

### Scheme 1. Composition of Jojoba Oil<sup>a</sup>



<sup>a</sup>*m* = 7, 9, 11, 13; *n* = 8, 10, 12, 14.

characteristics.<sup>4–9</sup> Jojoba oil is suited to a variety of numerous high-end applications such as cosmetics, pharmaceuticals, and foods<sup>10</sup> as well as high grade lubricating oil formulations.<sup>11,12</sup>

The oil from the jojoba plant has better thermal stability at high temperature compared to triacylglycerol (TAG) plant oils because glycerol, a component of the TAG, is readily destructible at high temperatures.<sup>13</sup> However, the low temperature performance, acid value, and oxidative stability of jojoba oil are not optimal when it is used as a lubricant base stock compared with those of mineral oil base stocks.<sup>11,14</sup> These physicochemical properties were found to be the limiting factors in the use of jojoba oil as a lubricant base stock.

The main obstacle to large scale use of jojoba oil is its cost and availability.<sup>15</sup> Different approaches have been considered for the production of cheap jojoba-like wax esters and their derivatives from inexpensive renewable resources such as vegetable oils<sup>16</sup> or fatty acids.<sup>17,18</sup> For example, synthesis routes using different catalysts such as Lewis acids,<sup>19–21</sup> ultrastable Y-zeolites,<sup>15</sup> or enzymes<sup>22</sup> are used to produce jojoba oil analogues from oleic acid and oleyl alcohol.

Different strategies are developed to produce cost-effective and high-performance chemicals based on these structures. In order to achieve desired functionality, target ester structures are synthesized and then chemically modified including changing the internal symmetry of the molecule, varying the chain length, or introducing branches at different positions in the chains.<sup>23</sup> However, fundamental studies on the structure–function relationships of these materials, and of esters in general, are lacking. In this regard, the Trent Centre for Biomaterials Research is conducting fundamental studies on the syntheses, crystallization, melt, polymorphism, solid fat content, viscosity, and modeling of structure and function of fatty esters and their derivatives.

The present contribution is one in a series of comprehensive studies carried out to elucidate the influence of structure on the physical properties, chain length, branching, symmetry, and functional groups of aliphatic mono-, di-, and triesters and their branched derivatives. Target pure ester compounds are synthesized and their functions are custom-engineered by structural modification at the fatty acid and/or alcohol chain level. This approach has been particularly successful in dramatically improving low temperature performance; for example, the branching of pure jojoba-like esters (JLEs) resulted in significant depression of crystallization temperatures—a sought-after property in lubricant formulations.<sup>24,25</sup>

In the present work, three jojoba-like esters incorporating either 9-decenoic acid and/or 9-decenol and oleic acid and/or oleyl alcohol were synthesized. 9-Decenoic acid or 9-decenol can be produced in a biorefinery process utilizing the ethenoic

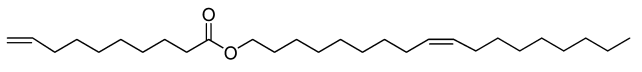
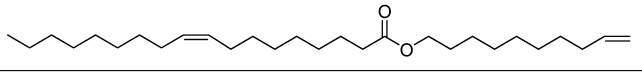
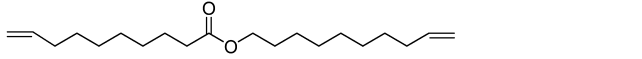
**Received:** October 31, 2012

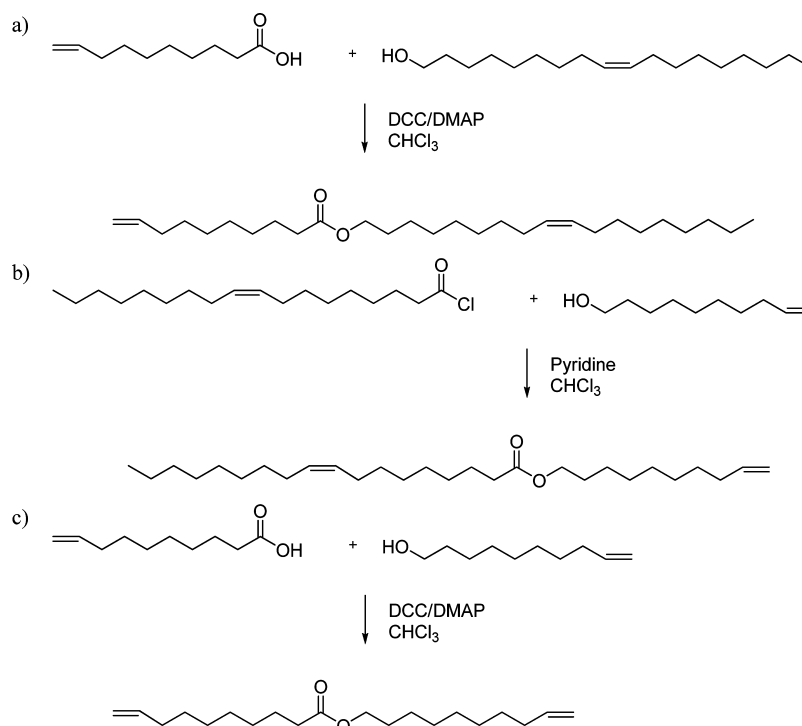
**Revised:** January 25, 2013

**Accepted:** January 30, 2013

**Published:** January 30, 2013

Scheme 2. Structure of Jojoba-like Esters (JLEs) with Terminal Double Bonds

octadec-9-enyl dec-9-enoate (JLE-28 <sub>1</sub> )	
dec-9-enyl oleate JLE-28 <sub>2</sub>	
dec-9-enyl dec-9-enoate (JLE-20)	

Scheme 3. Synthesis and Structures of Jojoba-like Esters (JLEs) with Terminal Double Bonds: (a) Octadec-9-enyl Dec-9-enoate (JLE 28<sub>1</sub>); (b) Dec-9-enyl Oleate (JLE 28<sub>2</sub>); (c) Dec-9-enyl Dec-9-enoate (JLE-20)

metathesis of highly unsaturated vegetable oils, and is a fatty acid/fatty alcohol whose unique terminal double bond structure has not before been investigated in monoester formulations. The model JLE molecules studied therefore contain three functional groups which can be used as the source of useful intermediates or final products. The terminal double bond can further be functionalized by carboxylation, amination, or epoxidation. The structures of the JLEs of this work are shown in Scheme 2.

The JLEs were characterized by <sup>1</sup>H NMR, and their purities were measured with high-performance liquid chromatography (HPLC). Differential scanning calorimetry (DSC), X-ray diffraction (XRD), and wide-line pulsed nuclear magnetic resonance (pNMR) were used to investigate their phase transition behaviors, crystal structures, microstructures, and solid fat contents (SFCs), respectively.

## 2. MATERIALS AND METHODS

**2.1. Materials.** The starting materials were sourced from oleic acid and erucic acid. Fatty materials used to make the compounds were oleyl alcohol (85% purity), oleoyl chloride (80% purity), 9-decenoic acid, 9-decen-1-ol, and propionic acid (Sigma-Aldrich). Other reagents used were pyridine, chloro-

form, dichloromethane, calcium hydride (CaH<sub>2</sub>), *N,N'*-dicyclohexylcarbodiimide (DCC), and 4-dimethylaminopyridine (DMAP), also purchased from Sigma-Aldrich. Hexane and ethyl acetate, from ACP Chemicals Inc. (Montreal, QC, Canada), were used without further treatment. Chloroform was distilled over calcium hydride.

**2.2. Synthesis Routes of Jojoba-like Esters with Terminal Double Bonds.** The jojoba-like esters with terminal double bonds were prepared from oleic acid, 9-decenoic acid, and their related alcohols by Steglich esterification<sup>26</sup> with 4-dimethylaminopyridine as the catalyst, or from their related chlorides with their alcohols in the presence of pyridine. Octadec-9-enyl dec-9-enoate (JLE 28<sub>1</sub>), dec-9-enyl oleate (JLE 28<sub>2</sub>), and dec-9-enyl dec-9-enoate (JLE-20) were prepared following the synthesis routes shown in parts a, b, and c, respectively, of Scheme 3.

**2.2.1. Synthesis of Octadec-9-enyl Dec-9-enoate (JLE-28<sub>1</sub>) (Scheme 3a).** To a solution of oleyl alcohol (10 mmol) in 20 mL of chloroform, 9-decenoic acid (10.1 mmol) and 4-dimethylaminopyridine (2 mmol) were added. This reaction mixture was cooled in an ice bath. Dicyclohexylcarbodiimide (11 mmol) in chloroform was added slowly, and the reaction mixture was stirred at room temperature overnight. Precipitated

dicyclohexylurea was removed by filtration. The organic phase was diluted with 60 mL of chloroform, then washed sequentially with water (3 × 50 mL), 4% NaHCO<sub>3</sub> (2 × 50 mL), and brine (3 × 50 mL), and then dried over Na<sub>2</sub>SO<sub>4</sub>. After filtration, the filtrate was rotary-evaporated and the residue was purified by column chromatography with ethyl acetate/hexanes = 1:40 to give a colorless oil.

Yield: 96%. <sup>1</sup>H NMR in CDCl<sub>3</sub>  $\sigma$  (ppm): 5.8 (1, m), 5.4 (2, m), 5.0 (2, dd), 4.1 (2, t), 2.3 (2, t), 2.0 (6, m), 1.6 (4, m), 1.4–1.2 (30, m), 0.9 (3, t). Purity: >99%.

**2.2.2. Synthesis of Dec-9-enyl Oleate (JLE-28<sub>2</sub>) (Scheme 3b).** To a solution of oleyl alcohol (10 mmol) in 30 mL of chloroform, oleoyl chloride (10 mmol) was added. Pyridine (12 mmol) was then added to the reaction solution dropwise. The reaction mixture was stirred at room temperature overnight. The reaction mixture was then diluted with 60 mL of chloroform. The organic layer was washed with water (3 × 50 mL), followed by 5% HCl (2 × 50 mL), water (2 × 50 mL), 4% NaHCO<sub>3</sub> (2 × 50 mL), and brine (3 × 50 mL). The organic layer was dried over Na<sub>2</sub>SO<sub>4</sub>. After filtration, chloroform was removed, and the residue was purified by column chromatography with ethyl acetate/hexanes = 1:40 to give a colorless oil.

Yield: 98%. <sup>1</sup>H NMR in CDCl<sub>3</sub>  $\sigma$  (ppm): 5.8 (1, m), 5.4 (2, m), 5.0 (2, dd), 4.1 (2, t), 2.3 (2, t), 2.0 (6, m), 1.6 (4, m), 1.4–1.2 (30, m), 0.9 (6, t). Purity: >99%.

**2.2.3. Synthesis of Dec-9-enyl Dec-9-enoate (JLE-20) (Scheme 3c).** Dec-9-enyl dec-9-enoate (JLE-20) was prepared from 9-decen-1-ol and 9-decenoic acid following the procedure described for the synthesis of JLE-28<sub>1</sub>. Pure JLE-20 was a colorless oil by column chromatography with ethyl acetate/hexanes = 1:50.

Yield: 93%. <sup>1</sup>H NMR in CDCl<sub>3</sub>  $\sigma$  (ppm): 5.8 (2, m), 5.0 (4, dd), 4.0 (2, t), 2.3 (2, t), 2.0 (4, m), 1.6 (4, m), 1.4–1.2 (18, m). Purity: >99%.

Note that these esters can also be prepared by the cross-metathesis of the oleic acid derivative, octadec-9-enoic acid octadec-9-enyl ester, with ethylene. The chain lengths of fatty acids and their derivatives can be shortened by their cross-metathesis reactions using ethylene,<sup>27–30</sup> butane, hexane,<sup>31</sup> or substitute alkenes.<sup>32–34</sup> The cross-metathesis with ethylene, so-called ethenolysis, is an important example, because ethylene is a favorable substrate of low cost and abundant supply.

**2.3. Analytical Methods.** All compounds were isolated and/or analyzed by HPLC and characterized by <sup>1</sup>H NMR spectroscopy. The physical measurements were run in at least triplicate. The reported values and uncertainties attached are the average and associated calculated standard deviations, respectively.

**2.3.1. High-Performance Liquid Chromatography (HPLC).** A Waters Alliance (Milford, MA, USA) e2695 HPLC system fitted with a Waters ELSD 2424 evaporative light scattering detector and a X-Bridge column (C18, 150 mm × 4.6 mm, 5.0  $\mu$ m, Waters Corp., Milford, MA, USA) was used for HPLC analysis. The mobile phase was a mixture of 40% chloroform:60% acetonitrile with a flow rate of 1 mL/min. Migration was studied using a 250 × 4 mm Betasil Diol-100 column (Thermo Hypersil-Keytone Inc., Bellefonte, PA, USA) in normal phase and isocratic mode. The temperature of the column was maintained at 30 °C (Alliance Column Heater, Waters Corp., Milford, MA, USA). ELSD nitrogen flow was set at 25 psi with nebulization and the drifting tube maintained at 12 and 60 °C, respectively. Gain was set at 500. The mobile

phase was heptane:isopropyl alcohol (90:10) run for 30 min at a flow rate of 0.5 mL/min. All solvents were HPLC grade and obtained from VWR International (Mississauga, ON, Canada).

**2.3.2. Nuclear Magnetic Resonance Spectroscopy (<sup>1</sup>H NMR).** One-dimensional <sup>1</sup>H NMR spectra were acquired on a Bruker Avance III 400 spectrometer ( $\nu$ (<sup>1</sup>H) = 400.22 MHz; Bruker BioSpin MRI GmbH, Karlsruhe, Germany) equipped with a 5 mm broad-band observe (BBO) probe. Spectra were acquired at 25 °C over a 16 ppm spectral window with a 1 s recycle delay, 32 transients. NMR spectra were Fourier transformed, phase corrected, and baseline corrected. Window functions were not applied prior to Fourier transformation. Chemical shifts were referenced relative to residual chloroform d1 solvent peaks.

**2.3.3. Differential Scanning Calorimetry (DSC).** DSC analysis was carried out on a Q200 model (TA Instruments, New Castle, DE, USA) equipped with a refrigerated cooling system (RCS 90, TA Instruments) under a nitrogen flow of 50 mL/min. Approximately 5.0–6.0 ( $\pm$ 0.1) mg of fully melted and homogeneously mixed sample was placed and hermetically sealed in an aluminum DSC pan. The samples were cooled from the melt (50 °C) to –90 °C and subsequently reheated to 70 °C at the same constant rate of 3.0 K/min to obtain the crystallization and melting profiles, respectively. “TA Universal Analysis” software coupled with a method developed in our group<sup>35</sup> was used to analyze the data and extract the main characteristics of the peaks. The sample was also cooled at a very low rate (0.1 K/min) then reheated at 1.0 K/min in order to account for the kinetic effects. The measurement temperatures are reported to a certainty of better than  $\pm$ 0.5 °C.

**2.3.4. Solid Fat Content (SFC) Determination.** The SFC measurements were performed on a Bruker Minispec mq 20 (Milton, Ontario, Canada) pNMR spectrometer equipped with a combined high and low temperature probe, and a temperature controller (Bruker BVT3000). Approximately 0.57  $\pm$  0.05 mL of fully melted sample was pipetted into the bottom of an NMR tube. The sample was subjected to the same thermal protocol as in the DSC (described in section 2.3.3). Note that SFC was not run at 0.1 K/min. The system was calibrated with highly unsaturated canola oil (with a heat capacity similar to that of the saturated oils, which do not crystallize until –20 °C). The accuracy of the measurement was determined to be greater than  $\pm$ 0.1 °C. In the low temperature region, the probe was supplied with N<sub>2</sub> gas, obtained by evaporating liquid nitrogen. The temperature was controlled to better than  $\pm$ 0.1 °C. SFC data were collected using Bruker’s Minispec plus V1.1 Rev. 05 software.

**2.3.5. Viscosity Measurements.** Sample viscosities were measured on a computer-controlled AR2000ex (TA Instruments, New Castle, DE, USA) using a standard-size recessed-end concentric cylinder (stator inner radius 15 mm and rotor outer radius 14 mm, SIN 545023.001). Temperature control was achieved by the Peltier effect with an accuracy of 0.1 °C. Viscosities of samples were measured from temperatures above each sample’s melting point up to 110 °C. The measurements were performed using shear rate/shear stress curves and constant temperature rates (0.1 and 3.0 K/min) with a constant shear rate (200 s<sup>–1</sup>). The two methods yielded measured viscosities in good agreement within the experimental uncertainty.

### 3. RESULTS AND DISCUSSION

**3.1. Products of Synthesis and Chemical Characterization.** JLE-28<sub>1</sub> (octadec-9-enyl dec-9-enoate) was prepared from oleyl alcohol and 9-decenoic acid, JLE-28<sub>2</sub> (dec-9-enyl oleate) was prepared from oleoyl chloride and 9-decen-1-ol, and JLE-20 (dec-9-enyl dec-9-enoate) was prepared from 9-decen-1-ol and 9-decenoic acid following the general procedure described in section 2.2. The pure JLEs were obtained as colorless oils by column chromatography. The purity of the JLEs as determined by HPLC was higher than 95%. The <sup>1</sup>H NMR spectra of the JLEs were consistent with the structures proposed. The column chromatography method and <sup>1</sup>H NMR data of JLEs are provided in the Supporting Information, listed in Table S1.

**3.2. Crystallization Behavior of Jojoba Wax-like Esters with Terminal Double Bond.** Typical cooling thermograms of purified JLE-28<sub>1</sub>, JLE-28<sub>2</sub>, and JLE-20 obtained at cooling rates of 0.1 and 3.0 K/min are shown in parts a and b, respectively, of Figure 1. The corresponding crystallization values are shown in Figure 1c. The crystallization data are provided in the Supporting Information, listed in Table S2.

As can be seen in Figure 1a,b, the cooling thermograms obtained at both 3.0 K/min (rapid cooling) and 0.1 K/min (slow cooling) of JLE-28<sub>1</sub> and JLE-28<sub>2</sub> have leading exotherms followed by a large crystallization event (P1 and P2 are indicated on the cooling trace of JLE-28<sub>2</sub> in Figure 1a), indicating a polymorphic behavior, whereas JLE-20 crystallized directly into its final phase with a single exotherm (Figure 1a,b). Comparison of thermodynamic data of JLE-28<sub>1</sub> and JLE-28<sub>2</sub> indicates that (a) the leading exotherm in JLE-28<sub>1</sub> has the lowest enthalpy (Table S2 in the Supporting Information), a sign that in this case less material is involved in the first liquid–solid transformation; (b) the main peak maximum in JLE-28<sub>1</sub> is lower, indicating that the main (second) phase formation in JLE-28<sub>1</sub> is less stable than that in JLE-28<sub>2</sub>; and (c) the presence of one exotherm in JLE-20 indicates that this material crystallizes directly into its most stable form without any polymorphic transformation.

There is a notable net temperature lag between the first and second transformations for both JLE-28<sub>1</sub> and JLE-28<sub>2</sub> samples. Differences in peak temperature values ( $T_{P1} - T_{P2}$ ) of 18.7 and 3.76 °C were obtained for JLE-28<sub>1</sub> and JLE-28<sub>2</sub>, respectively, when cooled at 3.0 K/min, and 20.1 and 4.7 °C, respectively, when cooled at 0.1 K/min. Such a large difference in crystal evolution between JLE-28<sub>1</sub> and JLE-28<sub>2</sub> must be due to quite different interactions, directional (dipole–dipole and CH $\cdots$ O bonds) and nondirectional (van der Waals), due to sizable differences in the structures of these molecules. These differences are probably quite sufficient to allow for a variety of transformation paths and phases to be realized.

The overall transformation path was not affected by the very different rates (30 times) used to crystallize the JLEs, suggesting that the crystallization process was only slightly affected by kinetics. Nevertheless, small differences can be observed between the DSC cooling thermograms obtained at 3.0 and 0.1 K/min.  $T_{On}$  values of the three JLEs shifted to lower temperatures by  $\sim 2.0$  °C, indicating that the formation of the first phase is only slightly affected by kinetics. Differences of 2.0, 1.4, and 0.4 °C in peak temperature of the main exotherm ( $T_{P2}$ ) were recorded for JLE-20, JLE-28<sub>1</sub>, and JLE-28<sub>2</sub>, respectively, indicating a gradual effect of kinetics on the formation path of the final phase in these JLEs.

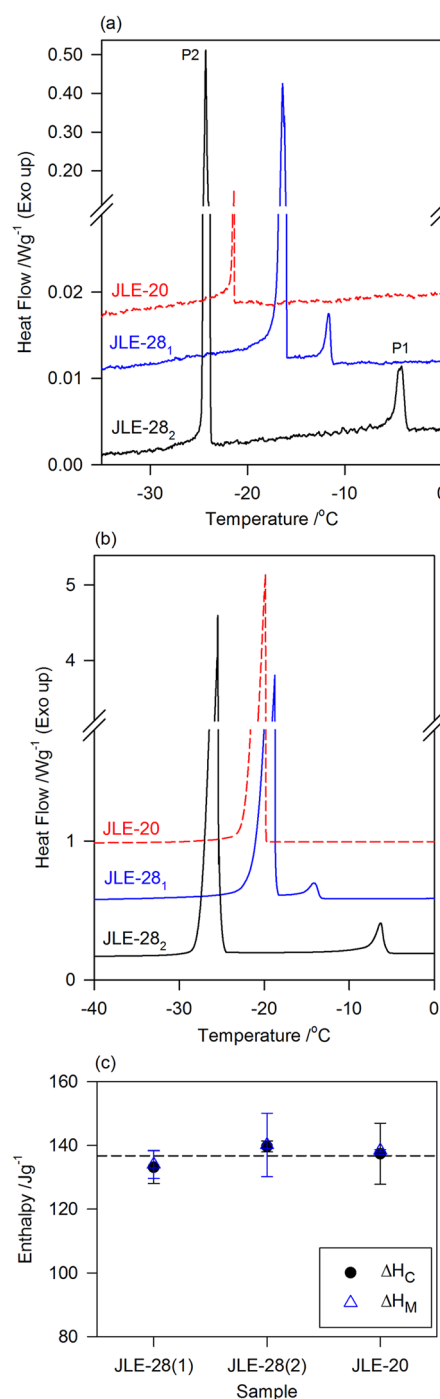


**Figure 1.** DSC cooling thermograms of the jojoba-like esters (JLEs) obtained at (a) 0.1 and (b) 3.0 K/min. (c) Total enthalpies of crystallization ( $\Delta H_C$ ) and melting ( $\Delta H_M$ ) of the JLEs.

The single exotherm of JLE-20 is very similar to the main crystallization peak of JLE-28<sub>1</sub>, albeit with a  $\sim 1$  °C lower onset ( $-19.47 \pm 0.766$  and  $-18.24 \pm 0.186$  °C, respectively). Interestingly, their total enthalpy of crystallization is the same (Figure 1c). When cooled rapidly, JLE-28<sub>1</sub> and JLE-20 displayed similarly shaped main exotherms with full width at half-maximum (fwhm) values of  $0.58 \pm 0.04$  and  $0.61 \pm 0.06$  °C, respectively, seemingly indicating similarity in crystal order and homogeneity, in contrast with JLE-28<sub>2</sub>, which has a fwhm twice as large ( $1.237 \pm 0.229$  °C), indicative of a relatively poor crystal order and lower homogeneity. Moreover, the onset and



peak temperatures of crystallization of JLE-20 differed only by  $\sim 1$  °C from those of the main peak of JLE-28<sub>1</sub> for both cooling rates (Figure 1a). Interestingly, JLE-20 presented a very small crystallization temperature span of  $0.1 \pm 0.1$  °C when cooled slowly, compared to  $2.9 \pm 0.1$  °C when cooled rapidly, which corresponds to a crystallization time of 1 min, whether JLE-20 is cooled rapidly or very slowly.

JLE-28<sub>1</sub> and JLE-28<sub>2</sub> display quite different transformation paths despite having the same number of carbons (Figure 1a,b). The onsets of crystallization in these samples occurred at relatively low temperatures with JLE-28<sub>2</sub> crystallizing earlier than JLE-28<sub>1</sub> whether cooled slowly or rapidly. Furthermore, the span of crystallization of JLE-28<sub>1</sub> is 3 times that of JLE-28<sub>2</sub> (Table S2 in the Supporting Information).

The structural differences between the two molecules are the length and nature of the chain attached to the C–O bond of the ester group in the molecule. JLE-28<sub>1</sub> has a chain (C9) with a terminal double bond, whereas JLE-28<sub>2</sub> has a long chain (C17), rigidly attached to the ester, with a cis double bond at C9. Therefore, the rotation of the molecules which is favored at the oxygen–carbon bond is quite different for the two molecules given the different structures of the hydrocarbon chain attached to each ester headgroup. The kink provided in the middle of the chain of JLE-28<sub>2</sub> is a conformation which will have more limited mobility and a higher entropic term when joining the growing surface compared to JLE-28<sub>1</sub>. Each molecule has therefore a unique expression of ester–ester, chain–chain, and chain–ester interactions which would explain the different transformation paths. The longer alkyl chain group in JLE-28<sub>2</sub> resulted in an earlier crystallization but in much more delayed polymorphic transformation compared to the enyl group in JLE-28<sub>1</sub>.

The reversal of the direction of the polar ester linking group influences both polarity and bending of the boomerang-shaped molecules and can explain differences observed in the onsets of crystallization of the two molecules. These differences probably originated at the nucleation stage and are due in large part to weaker  $\pi$ – $\pi$  interactions between the linking group of the bent-core molecules in JLE-28<sub>2</sub> compared to JLE-28<sub>1</sub>. Clearly, these considerations result in more of a barrier to crystallization for JLE-28<sub>1</sub> compared to JLE-28<sub>2</sub>, resulting in a lower first temperature peak ( $T_{p1}$ ) and enthalpy ( $\Delta H_1$ ) of crystallization in JLE-28<sub>1</sub> compared to JLE-28<sub>2</sub>.

The transformation from a low to a higher stability form (P1  $\rightarrow$  P2) was delayed in both JLEs because the rotational motion of the ester unit needed to achieve lower crystal energy is difficult, due to conformational reasons outlined above and to interactions with the neighboring chain. Despite a higher onset temperature, JLE-28<sub>2</sub> transformed into a more stable form much later than JLE-28<sub>1</sub> (18.7 °C compared to 3.76 °C in the rapid cooling, for example) because of easier rotations of its kinked chain as explained above. JLE-28<sub>1</sub> and JLE-20 have similar main exotherm characteristics and very close total enthalpies of crystallization, which may be evidence of similar phase types at low temperature. This is, however, an indication that the differences in phase trajectories observed in these JLEs are mainly driven by the subtle structural differences at the ester group level.

The analysis of the DSC cooling thermograms of the JLEs suggests clearly that the differences in crystallization behavior between the JLEs are mainly driven by the “asymmetry” about the ester group, i.e., the position of the central cis double bond relative to the singly bonded oxygen atom which allows the

rotations, and that the terminal double bonds have comparatively the same effect on the crystallization behaviors of the JLEs. Simultaneous consideration of the calorimetric and diffraction data will clarify the transformations occurring in the JLEs and will further reveal the nature of the phases developing.

### 3.3. Melting Behavior of the Jojoba Wax-like Esters.

Parts a and b, respectively, of Figure 2 present the heating thermograms of the JLEs obtained subsequent to cooling at 0.1 and 3.0 K/min, respectively. The corresponding melting data are provided in the Supporting Information, listed in Table S3.

Similar to crystallization, the heating thermograms of JLEs (Figure 2a,b) were only slightly affected by the cooling rate. The shapes of the endotherms were not affected, and the characteristic temperatures, including peak temperature, were shifted by less than 1 °C. Phase development as well as the type of phases involved was very similar, whether the JLEs were cooled rapidly or slowly. JLE-28<sub>2</sub> melted via three polymorphic transformations, two of which are very close (arrows in Figure 2a,b), whereas JLE-28<sub>1</sub> and JLE-20 recorded unique endotherms on melting. Overall, with the processing conditions applied, the esters crystallize and melt at temperatures below 0 °C regardless of the cooling rate and show very little polymorphic activity, with total enthalpies of melting similar to total enthalpies of crystallization (Figure 1c). Furthermore, the span of crystallization and span of melting are very close for each of these JLEs (Figure 2c in the case of rapid cooling), suggesting some reversibility in the transformation path of these esters, a characteristic which may be useful for developing new low temperature specialty oils such as lubricant-based products.

The endotherm observed for JLE-28<sub>1</sub> had an fwhm twice as wide as those of JLE-20 and JLE-28<sub>2</sub> (Table S3 in the Supporting Information), suggesting that it may be in fact the recording of a continuous overlap of two thermal events representing very close transformations. The two lowest endotherms observed in the heating thermogram of JLE-28<sub>2</sub> (Figure 2b) may be related to a polymorphic transformation and subsequent melting of a unique already formed phase or to the melting of two formed phases coexisting in the solid phase. Because there is only a difference of less than 2 °C between the two first endotherms of JLE-28<sub>2</sub> (see values of  $T_{p2}$  and  $T_{p3}$  in Table S3 in the Supporting Information), the transformation has probably involved a higher stability of the same polymorphic type formed during crystallization.

The heating thermogram of the fully symmetric JLE-20 displayed one single narrow endotherm which can be directly related to the melting of the unique crystal phase formed during the cooling cycle. Again, one can notice that the melting characteristics of this precrystallized form were not affected by the way it was crystallized, indicating that it is the most stable that can be obtained from the melt using a constant cooling rate.

As is commonly known, structural variations (acid and alcohol chain length, ester position, unsaturation) affect significantly the properties of esters. For example, melting temperatures ( $T_M$ 's) of molecules with the same number of carbon atoms decrease when the ester link is moved to less central locations along the molecule.<sup>36</sup> In the case of the molecules studied here, the number of carbons and position of the ester link relative to the center of the molecule would explain the differences observed in  $T_M$  values. JLE-20 which has alcohol and acid chains of the same length on either side of the

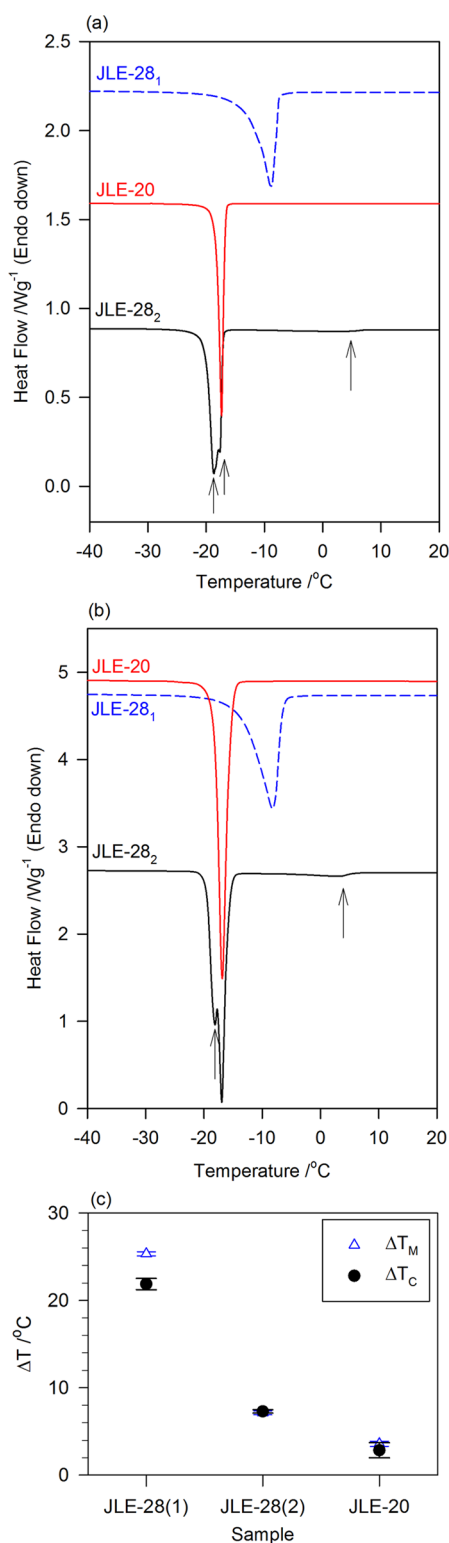


**Figure 2.** DSC heating thermograms of the jojoba-like esters (JLEs) obtained subsequent to cooling at (a) 0.1 and (b) 3.0 K/min. (c) Span of crystallization ( $\Delta T_C$ ) and span of melting ( $\Delta T_M$ ) of the JLEs subsequent to cooling at 3.0 K/min.

ester moiety (Scheme 1), has a  $T_M$  value much lower than  $T_M$ 's of the most stable forms of JLE-28<sub>1</sub> and JLE-28<sub>2</sub> (Table S3 in the Supporting Information). Obviously the effect of mass is superimposed to that of symmetry. However, JLE-20 has a  $T_M$  value almost identical to that of the main endotherm of JLE-

28<sub>2</sub>, which is attributable to its prevalent metastable form, suggesting that the effect of mass can be counterbalanced by the ester location. The difference in  $T_M$  between JLE-28<sub>1</sub> and JLE-28<sub>2</sub>, the molecules with the same number of carbons (28), points to the primordial role of the position of the C–O bond in asymmetrical molecules. It is therefore possible to not only lower the  $T_M$  of an ester by moving it away from a central location in the molecule but also further optimize its low temperature performance by choosing the direction of displacement of the ester group. In fact, it is the chain length of the whole ester group which predominantly dictates the behavior of the material.

**3.4. Solid Fat Content of JLEs.** The SFC (%) versus temperature curves obtained for the different purified ester compounds are shown in parts a and b of Figure 3 for the cooling cycle (3.0 K/min) and the heating cycle (3.0 K/min), respectively. The induction temperature of crystallization as measured by pNMR is presented in Figure 3c.

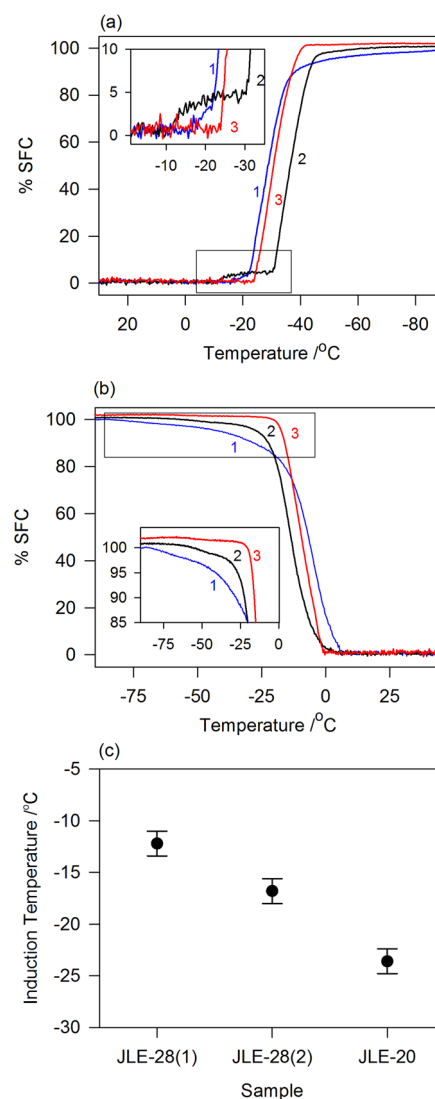


**Figure 3.** SFC (%) versus temperature curves of jojoba-like esters (JLEs) obtained during (a) cooling cycle (3.0 K/min) and (b) heating cycle (3.0 K/min). (c) Induction temperatures of crystallization of JLEs as measured by pNMR. Curves 1, 2, and 3 are for JLE-28<sub>1</sub>, JLE-28<sub>2</sub> and JLE-20, respectively.

As can be seen in Figure 3a, the solidification process and consequently the kinetics, as evidenced by SFC versus temperature of JLE-20, are dramatically simplified compared to those of JLE-28<sub>1</sub> and JLE-28<sub>2</sub>. Its SFC versus temperature curve is reminiscent of a single sigmoid which can be associated with an overall solidification occurring in one main step. The SFC versus temperature curves of JLE-28<sub>1</sub> and JLE-28<sub>2</sub> display two very distinct regions, the first of which covers only the early stages of solidification where less than 5% SFC was achieved (inset in Figure 3a). The application of the modified Avrami model, which takes into consideration the variances within the growth curve,<sup>37</sup> yielded two distinct temperature regions for JLE-28<sub>1</sub> and JLE-28<sub>2</sub>. In the modified Avrami model, each step is characterized by a constant growth rate and is described by an Avrami equation (a sigmoid) with an Avrami constant and Avrami exponent, applicable to nucleation, growth, and dimensionality of the crystallizing molecules over that step.

Obviously, JLE-20 crystallized via one overall crystallization step and JLE-28<sub>1,2</sub> crystallized in two main steps. The first sigmoid-shaped region observed in the SFC versus temperature curves of JLE-28<sub>1</sub> and JLE-28<sub>2</sub> (inset of Figure 3a) can be associated with the leading event observed in their DSC crystallization curves. The second sigmoid can be safely related to the main crystallization peak P2. JLE-28<sub>2</sub> achieved a higher percent SFC at the end of the first step (5% at −30 °C) than JLE-28<sub>1</sub> (3% at ~−20 °C). Note that the extension of the first step, i.e., the width of the first sigmoid, and the SFC induction temperature trends during the cooling cycle (Figure 3c) mirrored the fwhm of the first DSC exotherm and onset of crystallization, respectively. JLE-28<sub>2</sub> showed a measurable SFC at a temperature lower than JLE-28<sub>1</sub> by  $4.6 \pm 1.2$  °C, compared to a difference of  $7.6 \pm 0.21$  °C in DSC onset of crystallization. There was no SFC evidence of activated secondary nucleation, as only one segment has been identified in the main (second) sigmoid.

The SFC data strongly indicate that, overall, these compounds crystallize in a similar fashion but with subtle differences, corroborating findings from the DSC crystallization experiment. Therefore, the arguments proposed to explain the crystallization behavior as evidenced by DSC data apply to SFC versus temperature data.

Notwithstanding the variations mentioned before, these compounds form well-organized, plastic fats with predictable solidification behaviors. None of these JLEs achieved any SFC above −12 °C, and did fully achieve 100% SFC only below −40 °C, indicating they are viscous liquids at low temperatures enough to be useful for applications requiring low temperature performance such as cosmetic chemicals.

The trends observed for onset and offset temperatures, observed in the heating DSC cycle of JLEs (Figure 2b), were confirmed by SFC. The SFC versus temperature obtained on heating (Figure 3b) correlated very well with the DSC heating cycles as well. The SFC versus temperature curve of JLE-20 is also reminiscent of a single sigmoid, indicating a straight melting of a single phase, and mirrors perfectly its DSC counterpart. The polymorphic transformations observed in the DSC heating thermogram of JLE-28<sub>2</sub> were also apparent in its SFC counterpart. JLE-28<sub>1</sub> displayed also a two-stage melting SFC with an inflection point at ~−30 °C, the indication of a phase transformation occurring. This feature, which was not evident in the DSC heating data, is due to the nature of the NMR measurement technique which records the evolution with time (corresponding to temperature changes) of the NMR

signal ratio of protons in the solid and liquid states, respectively, and the details of which may not be accessible with DSC. This, however, explains the low slope of the left branch of the endotherm and the large width observed in the heating thermogram of JLE-28<sub>1</sub> and confirms our assumption of an overlap in the DSC recording of melting with a polymorphic transformation.

The central role that is played by the position of the hydroxyl groups in the JLEs, highlighted above, is supported by both the SFC cooling and heating curves. The SFC data confirmed that JLE-28<sub>1</sub>, which has its long kinked chain attached to the C—O single bond, is more prone to phase changes than JLE-28<sub>2</sub> during cooling due to both mass transfer limitations and rotation hindrances set by the rigid kink at the center of the chain. Conversely, when heated, transformations are easier in JLE-28<sub>2</sub> than in JLE-28<sub>1</sub> because both constraints are removed and only competition between the attractive forces and kinetic energy is at play.

**3.5. Viscosity of the JLEs.** JLE-28<sub>2</sub> and JLE-28<sub>1</sub> exhibited weakly Newtonian behavior over the examined range of shear rates, whereas JLE-20 presented weakly Newtonian behavior for temperatures below 20 °C and shear rate—shear stress curves with two distinct segments separated at a sharp singularity, or a critical shear rate ( $\dot{\gamma}_c$ ) indicating that these JLEs are rheologically relatively complex fluids. Shear stress—shear rate curves obtained at 0, 40, and 100 °C, typical of the flow behavior of the three JLEs, are presented in parts a, b, and c, respectively, of Figure 4.

The flow behavior of JLEs has been fitted with the Herschel–Bulkley equation (eq 1), a model commonly used to describe the general behavior of materials characterized by a yield stress.

$$\tau = \tau_0 + K\dot{\gamma}^n \quad (1)$$

where  $\dot{\gamma}$  denotes the shear stress,  $\tau_0$  is the yield stress below which there is no flow,  $K$  is the consistency index, and  $n$  is the power index.  $n$  depends on constitutive properties of the material. For shear-thickening fluids,  $n > 1$ , and for shear-thinning fluids,  $n < 1$ .

The application of eq 1 to shear rate—shear stress data of JLE-28<sub>1</sub> and JLE-28<sub>2</sub> ( $R^2 > 0.9999$ ) generated a yield stress of  $0.010 \pm 0.005$  Pa at all temperatures used, a value which is below the sensitivity limits of our equipment, indicating that these JLE fluids show no yield stress. The power law equation (eq 2) is therefore a valid model for these materials over the interval of shear rates used which would yield the same values for  $K$  and  $n$ . Note that in this investigation the shear rate range was optimized for torque (lowest possible is 10  $\mu\text{Nm}$ ) and velocity (maximum supplier suggested of 40 rad/s) and, therefore, it is not possible to state with confidence whether these materials display limiting viscosities in the limits of  $\dot{\gamma} \rightarrow \infty$ .

$$\tau = K\dot{\gamma}^n \quad (2)$$

or in terms of the apparent viscosity

$$\eta_{\text{app}} = K\dot{\gamma}^{n-1} \quad (3)$$

For Newtonian fluids,  $n = 1$  and  $K = \eta$  is the fluid viscosity.

Practically, these JLEs showed no yield stress, but their apparent viscosity increases slightly with the increasing shear rate. The power index ( $n$ ) values obtained for these systems by the Herschel–Bulkley (eq 1) and power law (eq 2) models, are

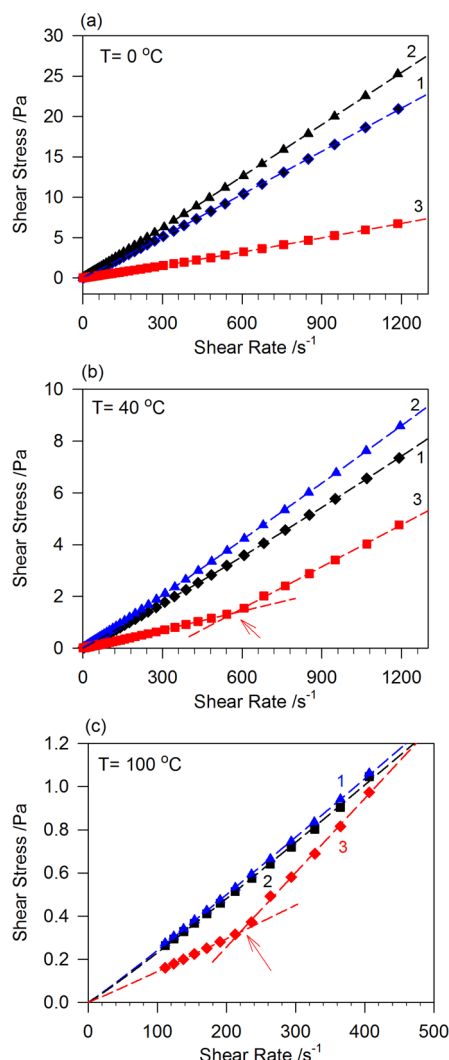


**Figure 4.** Selected shear stress–shear rate curves, typical of the flow behavior of the jojoba-like esters (JLEs). Measurements performed at (a) 0, (b) 40, and (c) 100 °C, respectively. Curves numbered 1, 2, and 3 are for JLE-28<sub>1</sub>, JLE-28<sub>2</sub>, and JLE-20, respectively.

slightly greater than unity, ranging from  $1.01$  to  $1.32 \pm 0.01$ , indicating weakly shear-thickening behavior. Fits to the Herschel–Bulkley (eq 1) model ( $n > 1$ ) are included in Figure 4.

The apparent viscosity determined for JLE-20 from the first segment ( $\eta_1$ ) is  $\sim 3$  times higher than that from the second ( $\eta_2$ ) at all measurement temperatures (the viscosity data are provided in the Supporting Information, listed in Table S4). A discontinuous increase in viscosity with increasing shear stress, such as that observed in JLE-20, is not uncommon and can be quite important.<sup>38,39</sup> This phenomenon studied by different techniques has even been quantitatively predicted for colloidal suspensions.<sup>40</sup>

Shear thickening, a less widely observed behavior than shear thinning, is observed in concentrated dispersions and so-called structured fluids. Typical examples of fluids showing shear-thickening behavior include thick suspensions and pastes, corn flour in water, etc. Such non-Newtonian flow behavior is thought to be caused by changes in the particle arrangements under shear.<sup>41</sup> Numerical simulations of the behavior of suspensions of particles provide a valuable tool for understanding complex rheological phenomena. Brady's research

group<sup>42–44</sup> developed a model which accounts for both the many-body interactions and the near-field lubrication effects. This model demonstrates that shear thickening is the result of a balance between viscous and interparticle forces. It predicts that when the viscous traction acting on a particle is sufficient to drive particles into contact, hydroclusters—groups of particles whose relative motions are restricted by lubrication stresses—will form and grow with increasing shear rate, increasing the hydrodynamic lubrication forces and resulting in thickening. Lubrication forces are short ranged and divergent at contact.<sup>45</sup> The model has been used successfully to simulate the flow behavior of suspensions. Very recently, Cheng et al.<sup>46</sup> reported the first direct experimental (combining fast confocal microscopy with simultaneous force measurements) verification of clusters of nearly touching particles that grow as the suspension thickens, consistent with the prediction that hydroclusters are responsible for shear thickening.

The very sharp singularity,  $\dot{\gamma}_c$  observed in JLE-20 (arrows in Figure 4b,c), indicates an abrupt change in the intermolecular interactions. It appears as if there was a critical “uncoupling” of preexisting molecular order in the liquid phase and a switch to a completely new and stronger interaction configuration, giving rise to a “viscosity switch”. This “viscosity” transition under shear may be explained by the very peculiar structure of the JLE-20 molecule. JLE-20 is a symmetrical molecule about a carbonyl center with two terminal double bonds and unlike JLE-28<sub>1,2</sub> has no extra hydrocarbon chain and, therefore, may lack the necessary van der Waals attractions which would ensure a continuous mass transfer under shear.

As demonstrated by Cheng et al.<sup>46</sup> in the case of colloidal suspensions, shear thickening is dominated by hydrodynamic interactions rather than frictional contacts between particles and that changes in layering and in-layer order may not have contributed to shear thickening. As they have also found, entropic contributions to viscosity may be negligible in the shear-thickening regime.

The shear-thickening systems are dominated by hydrodynamic interactions rather than frictional contacts between particles. The critical shear rate ( $\dot{\gamma}_c$ ) decreased exponentially with temperature ( $R^2 = 0.9955$ , figure not shown), indicating that the effect that gave rise to the singularity becomes less effective as temperature increases, understandably as kinetic energy counterbalances the intermolecular interactions. As postulated by Chow et al.,<sup>47</sup> shear thickening occurs when stress fluctuations cannot relax, i.e., when Brownian forces are no longer able to restore shear-induced perturbations to the equilibrium microstructure on the time scale of the shear flow. The ratio of the applied shear rate  $\dot{\gamma}$  to the inverse of the Brownian relaxation time (the so-called Peclet number) of the system is used as a measure of how far the system's microstructure is driven from equilibrium.<sup>45</sup>

Viscosity versus temperature curves of JLE-28<sub>1</sub>, JLE-28<sub>2</sub>, and JLE-20 obtained using the ramp procedure at a constant shear rate of  $200 \text{ s}^{-1}$  (section 2.3.5) are presented in Figure 5. Viscosities of JLE-28<sub>2</sub> are higher than those of JLE-28<sub>1</sub>, which in turn are higher than those of JLE-20 at any given temperature. Note that the viscosity differences are larger at low temperatures than at high temperatures.

The experimental viscosity–temperature data were analyzed using the generalized form of the van Velzen expression (GvVE, eq 4), a model found to be more appropriate than other comparative equations. The fit parameters ( $n$  and  $A$ ) are provided in the Supporting Information, listed in Table S5.



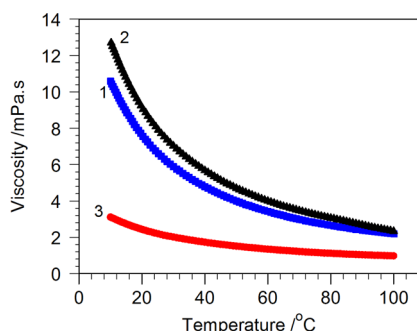


**Figure 5.** Viscosity versus temperature curves of jojoba-like esters (JLEs) obtained using the ramp procedure at a constant shear rate of  $200 \text{ s}^{-1}$ . 1, JLE-28<sub>1</sub>; 2, JLE-28<sub>2</sub>; 3, JLE-20.

$$\ln(\eta) = A \left( -1 + \frac{1}{T^n} \right) \quad (4)$$

The magnitude of  $n$  (related to the activation energy) is an indication of the difficulty of transfer of molecules through the liquid matrix. The value of  $n$  for JLE-28<sub>1</sub> is higher than that for JLE-28<sub>2</sub>, and they are both lower than that for JLE-20 (Table S5 in the Supporting Information), suggesting that structural complexity involved with the bent geometry of the ester is more relevant to the rheology of the fluid JLEs than the asymmetry about the C–O bond. However, the position of the hydrocarbon chains relative to the C–O bond is significant in determining differences between JLE-28<sub>1</sub> and JLE-28<sub>2</sub>. The parameter  $A$  of JLE-28<sub>2</sub> was higher than that of JLE-28<sub>1</sub>, and both are higher than that of JLE-20, as expected from the respective magnitudes of their respective viscosity versus temperature curves (Figure 5).

#### 4. CONCLUSIONS

Three jojoba-like esters (JLEs) with shortened chain lengths and terminal double bonds were synthesized from fatty acids and fatty alcohols. Octadec-9-enyl dec-9-enoate and dec-9-enyl oleate were designed and synthesized based on the asymmetrization of the fully symmetrical dec-9-enyl dec-9-enoate molecule. Their crystallization and melt behaviors were elucidated as a function of chain length, symmetry, and position of functional groups relative to the ester headgroup. DSC and SFC data indicated clearly that the length of the terminal alkyl chain and orientation of the linking group in the side chains of the bent-core molecules play an important role in the phase development of the JLEs. The transformation behavior of these JLEs is explained by the competition of the intermolecular  $\pi$ – $\pi$  attractions due to ester groups which promote crystallization, with the restriction to participation of molecules in crystallization due to structural complexity of the molecule (position of the central cis double bond relative to the C–O–C bond of the ester group and rotation hindrance). The monoesters demonstrated very little hysteresis on melt/cool cycling, suggesting that they are materials which can be exploited well as lubricants and waxes in applications such as greases, cosmetics, and pharmaceuticals. Furthermore, the findings highlight relatively simple, single-molecule esters, much easier to produce from cheap fatty acid feedstock with astonishingly low onsets of crystallization—a sought-after property of lubricant additives.

## ■ ASSOCIATED CONTENT

### Supporting Information

Figure S1,  $^1\text{H}$  NMR spectra of octadec-9-enyl dec-9-enoate (JLE 28<sub>1</sub>), dec-9-enyl oleate (JLE 28<sub>2</sub>), and dec-9-enyl dec-9-enoate (JLE-20). Table S1, synthesis and  $^1\text{H}$  NMR characterization data of jojoba-like esters (JLEs): JLE-28<sub>1</sub>, JLE-28<sub>2</sub>, and JLE-20. Table S2, onset ( $T_{\text{On}}$ ), peak ( $T_{\text{P1,2}}$ ), offset ( $T_{\text{Off}}$ ), and enthalpy ( $\Delta H_{\text{C}}$ ) of crystallization of JLEs with terminal double bonds: JLE-28<sub>1</sub>, JLE-28<sub>2</sub>, and JLE-20. Table S3, onset, peak, offset, and enthalpy of melting of JLEs with terminal double bonds: JLE-28<sub>1</sub>, JLE-28<sub>2</sub>, and JLE-20. Table S4, viscosity of JLE-20 obtained from fits of the shear rate–shear stress linear segments data. Table S5, parameters of fit of JLEs with terminal double bonds to the generalized van Velzen equation (GvVE, eq 4). This material is available free of charge via the Internet at <http://pubs.acs.org>.

## ■ AUTHOR INFORMATION

### Corresponding Author

\*Tel.: (705) 748-1011, ext 6105. Fax: (705) 748-1652. E-mail: [sureshnarine@trentu.ca](mailto:sureshnarine@trentu.ca).

### Notes

The authors declare no competing financial interest.

## ■ ACKNOWLEDGMENTS

The financial support of Elevance Renewable Sciences, NSERC, Grain Farmers of Ontario, GPA-EDC, Industry Canada, and Trent University is gratefully acknowledged.

## ■ REFERENCES

- (1) Battersby, N. S.; Ciccognani, D.; Evans, M. R.; King, D.; Painter, H. A.; Peterson, D. R.; Starkey, M. An 'inherent' biodegradability test for oil products: Description and results of an international ring test. *Chemosphere* **1999**, 38 (14), 3219–3235.
- (2) Battersby, N. S. The biodegradability and microbial toxicity testing of lubricants—some recommendations. *Chemosphere* **2000**, 41 (7), 1011–1027.
- (3) Santos, J. C. O.; Santos, I. M. G.; Conceicao, M. M.; Porto, S. L.; Trindade, M. F. S.; Souza, A. G.; Prasad, S.; Fernandes, V. J.; Araujo, A. S. Thermoanalytical, kinetic and rheological parameters of commercial edible vegetable oils. *J. Therm. Anal. Calorim.* **2004**, 75 (2), 419–428.
- (4) Le Dréau, Y.; Dupuy, N.; Gaydou, V.; Joachim, J.; Kister, J. Study of jojoba oil aging by FTIR. *Anal. Chim. Acta* **2009**, 642 (1–2), 163–170.
- (5) Wisniak, J. Potential uses of jojoba oil and meal—a review. *Ind. Crops Prod.* **1994**, 3 (1–2), 43–68.
- (6) Miwa, T. K. Jojoba oil wax esters and derived fatty acids and alcohols: gas chromatographic analyses. *J. Am. Oil Chem. Soc.* **1971**, 48, 259–264.
- (7) Busson-Breyse, J.; Farines, M.; Soulier, J. Jojoba wax: Its esters and some of its minor components. *J. Am. Oil Chem. Soc.* **1994**, 71 (9), 999–1002.
- (8) Tobares, L.; Frati, M.; Guzmán, C.; Maestri, D. Agronomical and chemical traits as descriptors for discrimination and selection of jojoba (*Simmondsia chinensis*) clones. *Ind. Crops Prod.* **2004**, 19 (2), 107–111.
- (9) Binman, S.; Belfer, S.; Shani, A. Functionalization at the double-bond region of jojoba oil. 7. Chemical binding of jojoba liquid wax to polystyrene resins. *J. Am. Oil Chem. Soc.* **1996**, 73 (9), 1075–1081.
- (10) Patel, S.; Nelson, D. R.; Gibbs, A. G. Chemical and physical analyses of wax ester properties. *J. Insect Sci. (Madison, WI, U. S.)* **2001**, No. 1.4, Available online: [insectscience.org/1.4](http://insectscience.org/1.4).
- (11) Bhatia, V. K.; Chaudhry, A.; Sivasankaran, G. A.; Bisht, R. P. S.; Kashyap, M. Modification of jojoba oil for lubricant formulations. *J. Am. Oil Chem. Soc.* **1990**, 67 (1), 1–7.

- (12) Bisht, R. P. S.; Sivasankaran, G. A.; Bhatia, V. K. Additive properties of jojoba oil for lubricating oil formulations. *Wear* **1993**, *161* (1–2), 193–197.
- (13) Gryglewicz, S.; Piechocki, W.; Gryglewicz, G. Preparation of polyol esters based on vegetable and animal fats. *Bioresour. Technol.* **2003**, *87* (1), 35–39.
- (14) Tobares, L.; Guzmán, C.; Maestri, D. Effect of the extraction and bleaching processes on jojoba (*Simmondsia chinensis*) wax quality. *Eur. J. Lipid Sci. Technol.* **2003**, *105* (12), 749–753.
- (15) Sanchez, N.; Martinez, M.; Aracil, J.; Corma, A. Synthesis of oleyl oleate as a jojoba oil analog. *J. Am. Oil Chem. Soc.* **1992**, *69* (11), 1150–1153.
- (16) Campanella, A.; Rustoy, E.; Baldessari, A.; Baltanás, M. A. Lubricants from chemically modified vegetable oils. *Bioresour. Technol.* **2010**, *101* (1), 245–254.
- (17) Kalscheuer, R.; Stoveken, T.; Luftmann, H.; Malkus, U.; Reichelt, R.; Steinbuchel, A. Neutral Lipid Biosynthesis in Engineered *Escherichia coli*: Jojoba Oil-Like Wax Esters and Fatty Acid Butyl Esters. *Appl. Environ. Microbiol.* **2006**, *72* (2), 1373–1379.
- (18) Wahlen, B. D.; Oswald, W. S.; Seefeldt, L. C.; Barney, B. M. Purification, Characterization, and Potential Bacterial Wax Production Role of an NADPH-Dependent Fatty Aldehyde Reductase from *Marinobacter aquaeolei* VT8. *Appl. Environ. Microbiol.* **2009**, *75* (9), 2758–2764.
- (19) Martinez, M.; Torrano, E.; Aracil, J. Synthesis of esters of high molecular weight. An analogue of jojoba oil. A statistical approach. *Ind. Eng. Chem. Res.* **1988**, *27* (11), 2179–2182.
- (20) Ieda, N.; Mantri, K.; Miyata, Y.; Ozaki, A.; Komura, K.; Sugi, Y. Esterification of Long-Chain Acids and Alcohols Catalyzed by Ferric Chloride Hexahydrate. *Ind. Eng. Chem. Res.* **2008**, *47* (22), 8631–8638.
- (21) Mantri, K.; Komura, K.; Sugi, Y. Efficient esterification of long chain aliphatic carboxylic acids with alcohols over  $\text{ZrOCl}_2 \cdot 8\text{H}_2\text{O}$  catalyst. *Synthesis* **2005**, *12*, 1939–1944.
- (22) Garcia, T.; Martinez, M.; Aracil, J. Enzymatic synthesis of an analogue of jojoba oil: Optimization by statistical analysis. *Enzyme Microb. Technol.* **1993**, *15* (7), 607–611.
- (23) Brown, M.; Fotheringham, J. D.; Hoyes, T. J.; Mortier, R. M.; Orszulik, S. T.; Randles, S. J.; Stroud, P. M. *Synthetic Base Fluids*; Springer-Verlag: Berlin, 2010; pp 35–74.
- (24) Bouzidi, L.; Li, S.; Di Biase, S.; Rizvi, S. Q.; Narine, S. S. Lubricating and waxy esters. I. Synthesis, crystallization, and melt behavior of linear monoesters. *Chem. Phys. Lipids* **2012**, *165* (1), 38–50.
- (25) Bouzidi, L.; Li, S.; Di Biase, S.; Rizvi, S.; Dawson, P.; Narine, S. S. Lubricating and Waxy Esters. 2. Synthesis, Crystallization, and Melt Behavior of Branched monoesters. *Ind. Eng. Chem. Res.* **2012**, *51* (45), 14892–14902, DOI: 10.1021/ie3016472.
- (26) Neises, B.; Steglich, W. Simple Method for the Esterification of Carboxylic Acids. *Angew. Chem., Int. Ed.* **1978**, *17* (7), 522–524.
- (27) Burdett, K. A.; Harris, L. D.; Margl, P.; Maughon, B. R.; Mokhtar-Zadeh, T.; Saucier, P. C.; Wasserman, E. P. Renewable monomer feedstocks via olefin metathesis: Fundamental mechanistic studies of methyl oleate ethenolysis with the first-generation Grubbs catalyst. *Organometallics* **2004**, *23* (9), 2027–2047.
- (28) Forman, G. S.; Bellabarba, R. M.; Tooze, R. P.; Slawin, A. M. Z.; Karch, R.; Winde, R. Metathesis of renewable unsaturated fatty acid esters catalysed by a Phoban-indenylidene ruthenium catalyst. *J. Organomet. Chem.* **2006**, *691* (24–25), 5513–5516.
- (29) Schrodli, Y.; Ung, T.; Vargas, A.; Mkrtumyan, G.; Lee, C. W.; Champagne, T. M.; Pederson, R. L.; Hong, S. H. Ruthenium olefin metathesis catalysts for the ethenolysis of renewable feedstocks. *Clean: Soil, Air, Water* **2008**, *36* (8), 669–673.
- (30) Zlatanovic, A.; Petrovic, Z. S.; Dusek, K. Structure and properties of triolein-based polyurethane networks. *Biomacromolecules* **2002**, *3* (5), 1048–1056.
- (31) Patel, J.; Mujcinovic, S.; Jackson, W. R.; Robinson, A. J.; Serelis, A. K.; Such, C. High conversion and productive catalyst turnovers in cross-metathesis reactions of natural oils with 2-butene. *Green Chem.* **2006**, *8* (5), 450–454.
- (32) Miao, X.; Malacea, R.; Fischmeister, C.; Bruneau, C.; Dixneuf, P. H. Ruthenium-alkylidene catalysed cross-metathesis of fatty acid derivatives with acrylonitrile and methyl acrylate: a key step toward long-chain bifunctional and amino acid compounds. *Green Chem.* **2011**, *13* (10), 2911–2919.
- (33) Jacobs, T.; Rybak, A.; Meier, M. A. R. Cross-metathesis reactions of allyl chloride with fatty acid methyl esters: Efficient synthesis of alpha,omega-difunctional chemical intermediates from renewable raw materials. *Appl. Catal., A: Gen.* **2009**, *353* (1), 32–35.
- (34) Miao, X. W.; Dixneuf, P. H.; Fischmeister, C.; Bruneau, C. A green route to nitrogen-containing groups: the acrylonitrile cross-metathesis and applications to plant oil derivatives. *Green Chem.* **2011**, *13* (9), 2258–2271.
- (35) Bouzidi, L.; Boodhoo, M.; Humphrey, K. L.; Narine, S. S. Use of first and second derivatives to accurately determine key parameters of DSC thermographs in lipid crystallization studies. *Thermochim. Acta* **2005**, *439* (1–2), 94–102.
- (36) Patel, S.; Nelson, D. R.; Gibbs, A. G. Chemical and physical analyses of wax ester properties. *J. Insect Sci.* **2001**, *1*, 4.
- (37) Narine, S.; Humphrey, K.; Bouzidi, L. Modification of the Avrami model for application to the kinetics of the melt crystallization of lipids. *J. Am. Oil Chem. Soc.* **2006**, *83* (11), 913–921.
- (38) Barnes, H. A. Shear-thickening (“dilatancy”) in suspensions of nonaggregating solid particles dispersed in Newtonian liquids. *J. Rheol.* **1989**, *33* (2), 329–366.
- (39) Boersma, W. H.; Laven, J.; Stein, H. N. Shear thickening (dilatancy) in concentrated dispersions. *AIChE J.* **1990**, *36* (3), 321–332.
- (40) Maranzano, B. J.; Wagner, N. J. The effects of particle-size on reversible shear thickening of concentrated colloidal dispersions. *J. Chem. Phys.* **2001**, *114* (23), 10514–10527.
- (41) Brown, E.; Jaeger, H. M. Through Thick and Thin. *Science* **2011**, *333* (6047), 1230–1231.
- (42) Durlofsky, L.; Brady, J. F.; Bossis, G. Dynamic simulation of hydrodynamically interacting particles. *J. Fluid Mech.* **1987**, *180*, 21–49.
- (43) Brady, J. F.; Bossis, G. Stokesian Dynamics. *Annu. Rev. Fluid Mech.* **1988**, *20* (1), 111–157.
- (44) Brady, J. F.; Phillips, R. J.; Lester, J. C.; Bossis, G. Dynamic simulation of hydrodynamically interacting suspensions. *J. Fluid Mech.* **1988**, *195*, 257–280.
- (45) Chen, D. T. N.; Wen, Q.; Janmey, P. A.; Crocker, J. C.; Yodh, A. G. Rheology of Soft Materials. *Annu. Rev. Condens. Matter Phys.* **2010**, *1* (1), 301–322.
- (46) Cheng, X.; McCoy, J. H.; Israelachvili, J. N.; Cohen, I. Imaging the Microscopic Structure of Shear Thinning and Thickening Colloidal Suspensions. *Science* **2011**, *333* (6047), 1276–1279.
- (47) Chow, M. K.; Zukoski, C. F. Gap size and shear history dependencies in shear thickening of a suspension ordered at rest. *J. Rheol.* **1995**, *39* (1), 15–32.